Numerical methods in General Relativity (and possible other theories of gravity...)

European Einstein Toolkit Meeting 2024

Isabel Cordero-Carrión
University of Valencia (Spain)

Huge thanks to Bruno Giacomazzo and Peter Diener for their talks.

Contents:

→ Don't forget the details: EoS and numerical simulations.

→ Numerical vs physical resistivity: MIRK methods for the RRMHD equations.

→ Adding more ingredients: MIRK methods for the neutrino transport equations (M1 scheme) in supernovae simulations.

→ Numerical resolution of elliptic equations: at least for initial data.
→ Your hyperbolic sector has (gravitational) waves: RK methods and stability.

→ Black hole singularities in your numerical grid.

And everything is **coupled**...

Oscillation modes in HMNS (early postmerger)

[Toni Font et al.]

GW signal divided in three distinct phases:
inspiral, merger, postmerger oscillations

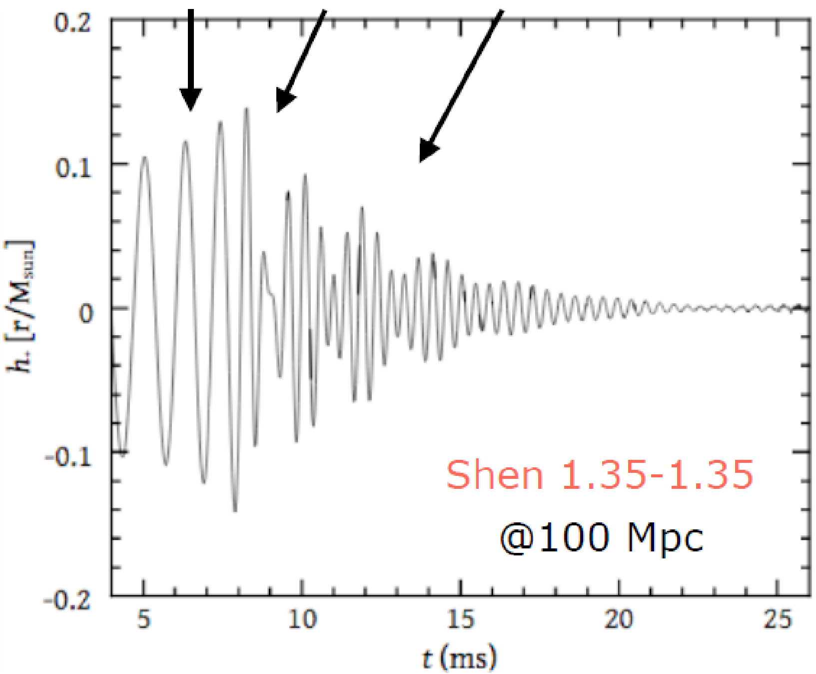

Stergioulas+ (2011)

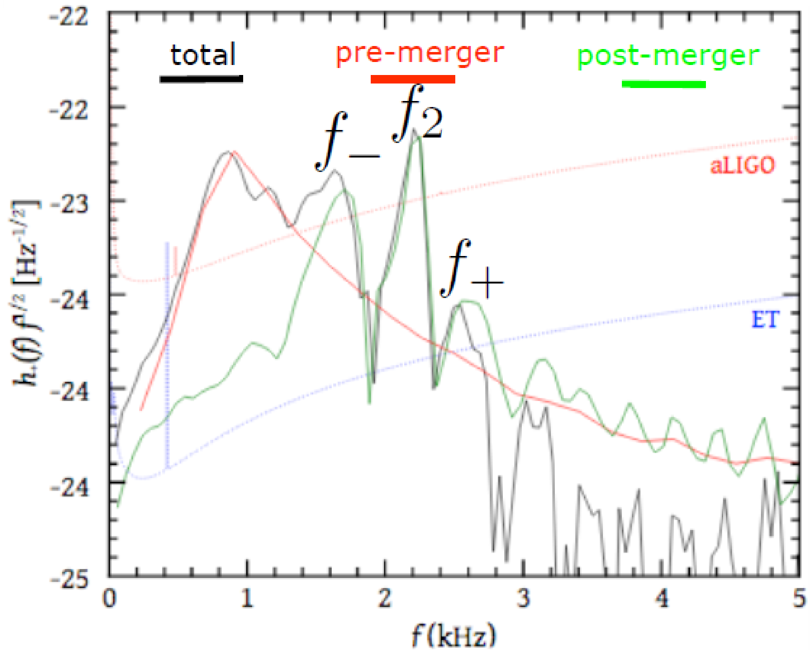

Triplet of frequencies identified in GW spectrum.

Future GW observations may extract f_2 & f_0

GW **asteroseismology** with post-merger remnant to **constrain the EOS.**

$f_{\rm peak} = f_2$ fundamental l=m=2 f-mode oscillation

$f_- = f_2 - f_0$

$f_+ = f_2 + f_0$

quasilinear combination tones

Constraining the EoS

Bauswein+ (2012): peak frequency of (1.35−1.35)$M_\odot$ BNS merger correlates with the radius of a 1.6$M_\odot$ nonrotating NS in an EoS-independent manner.

Similar relations found for other binary masses and other radii ($R_{1.35}$ or $R_{1.8}$)

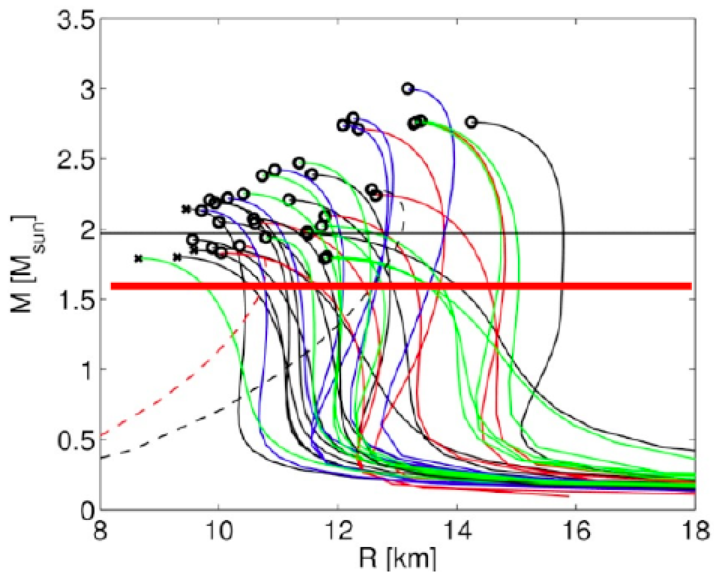

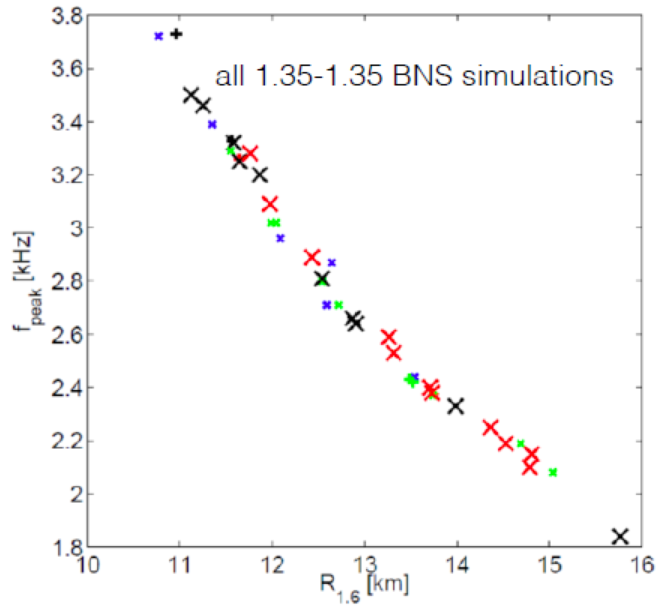

A potential measurement of f_{peak} from postmerger signal can be used to obtain an estimate on $R_{1.6}$, a quantity that can be used to directly constrain the EoS.

The smaller the scatter (<200 m) the smaller the error in radius measurement.

BNS mergers with hadron-quark phase transitions

Bauswein+ (2019) identified an observable imprint of a first-order hadron-quark PT at supranuclear densities on the GW emission of BNS mergers.

Dominant postmerger GW frequency f_{peak} may exhibit a significant deviation from an empirical relation between f_{peak} and tidal deformability if a first-order PT leads to the formation of a stable extended quark matter core in the postmerger remnant.

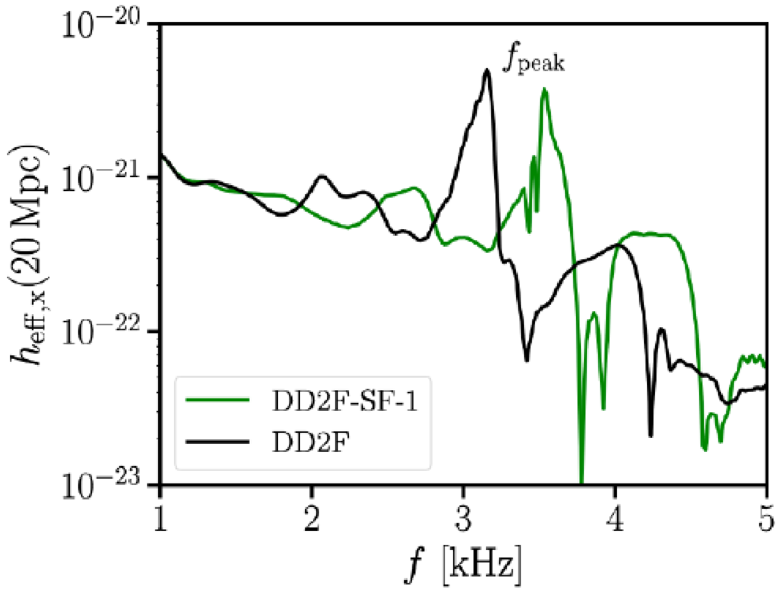

(Bauswein+ 2019)

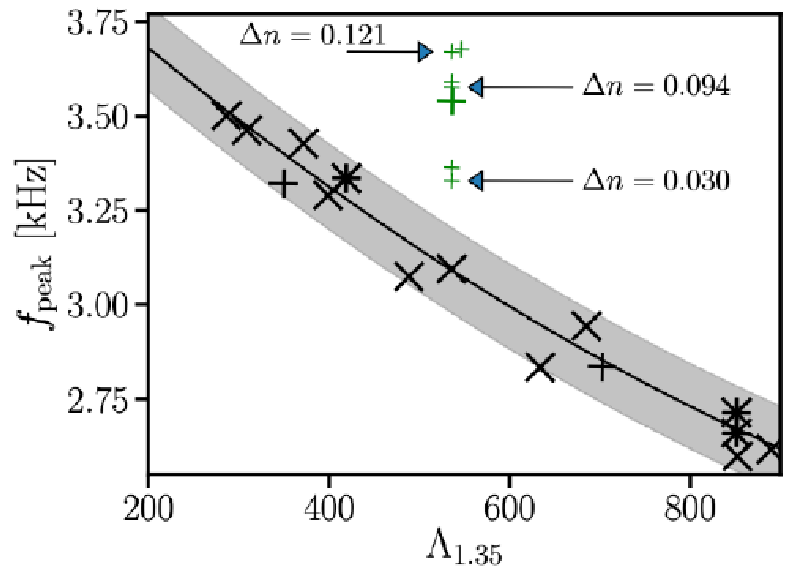

Green + : DD2F-SF EoS (PT to deconfined quarks)

Black markers: purely hadronic EoS

EoS from Wroclaw group (Fischer+ 2018, Bastian+ 2018)

→ Could this shift in the frequency be explained by a different reason?
→ Could the anomalous dynamics be triggered by a non-convex EoS?

Non-convexity of isentropes in the p-rho plane: compressive rarefaction waves and expansive shocks. Classical fluid dynamics, the convexity is determined by the fundamental derivative:

$$\mathcal{G}_{(C)} \equiv -\frac{1}{2} V \frac{\frac{\partial^2 p}{\partial V^2}}{\frac{\partial p}{\partial V}} \qquad \mathcal{G}_{(C)} = 1 + \frac{\partial \log c_s}{\partial \log \rho} = \frac{1}{2}\left(1 + \Gamma_1 + \frac{\partial \log \Gamma_1}{\partial \log \rho}\right)$$

(all derivatives computed at constant entropy)

Γ_1 adiabatic index. Characterizes stiffness of EoS at a given density, showing a local maximum above nuclear matter density.

Bethe (1942), Zel'dovich (1946) and Thompson (1971) (BZT) fluids exhibit negative values for the fundamental derivative.

Relativistic fluids [Ibáñez, Cordero-Carrión et al. (2013)]: extension to the relativistic case, introducing the relativistic fundamental derivative:

$$\mathcal{G}_{(R)} = \mathcal{G}_{(C)} - \frac{3}{2}\, c^2_{s(R)}$$

$$p = (\Gamma - 1)\rho\epsilon \qquad \Gamma = \gamma_0 + (\gamma_1 - \gamma_0)e^{-\frac{(\rho-\rho_1)^2}{\sigma^2}}$$

Ibáñez+ 2018

Non-convex dynamics (toy model EoS)

Convex dynamics (Ideal gas EoS)

EoS broadly used in numerical simulations of CCSN and BNS mergers display regions where adiabatic index is not monotonic → non-convex regions.

Good news: you can use standard numerical methods.

Illustrative example: effect on BNS mergers with a phenomenological toy-model EoS

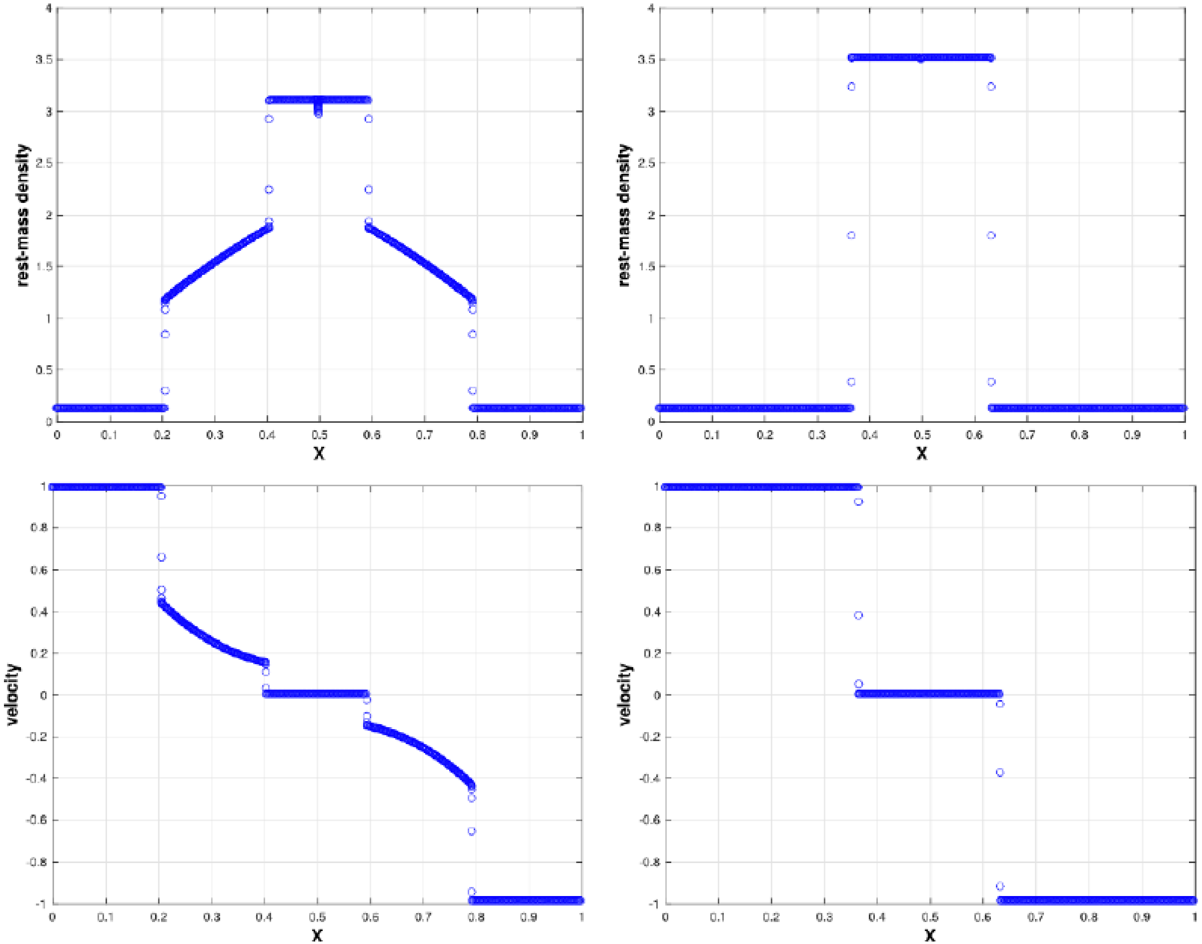

Empirical universal relations affected by non-convex dynamics

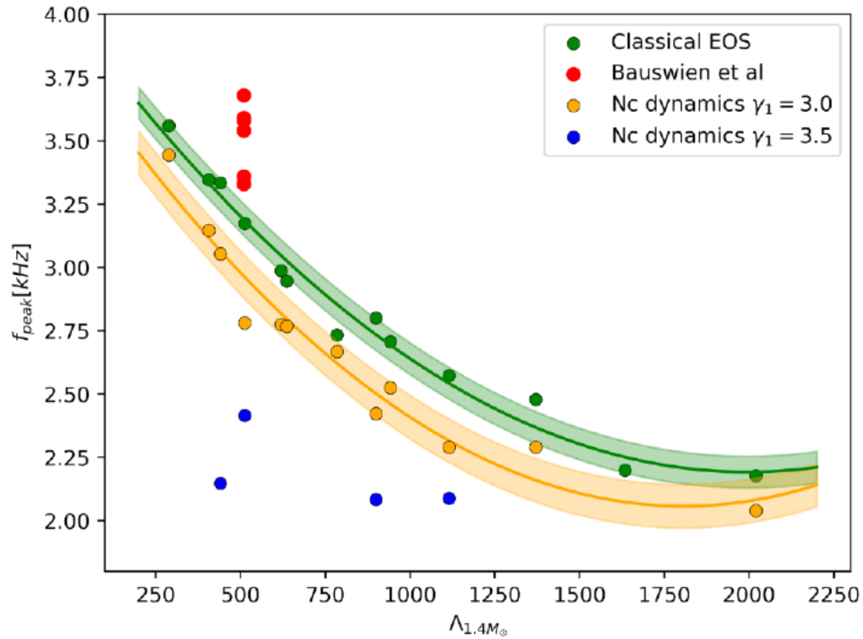

Significant shifts in frequency observed for f2 mode: as large as ~500 Hz for some choice of toy-model EoS parameters.

Do these findings hold for realistic EoS?

Rivieccio+ (2024)

This is not really the end of the story [Ibáñez, Cordero-Carrión et al. (2015)]: the relativistic fundamental derivative has corrections due to the presence of intense magnetic fiels.

$$\tilde{\mathcal{G}}_{\mathrm{M}} := \tilde{\mathcal{G}} + F,$$

where

$$F := \frac{3}{2} W_s^{-4} \left(\frac{c_a^{\,2}/a_s^{\,2} - R}{1 - R} \right).$$

In the previous expressions, $R := \frac{\mathcal{B}^2}{\mathcal{E}a^2}$, and $c_a^{\,2} := \frac{b^2}{\mathcal{E}}$

Also, take care about the treatment of thermal effects in postmerger BNS merger with hybrid EoS vs tabulated EoS:

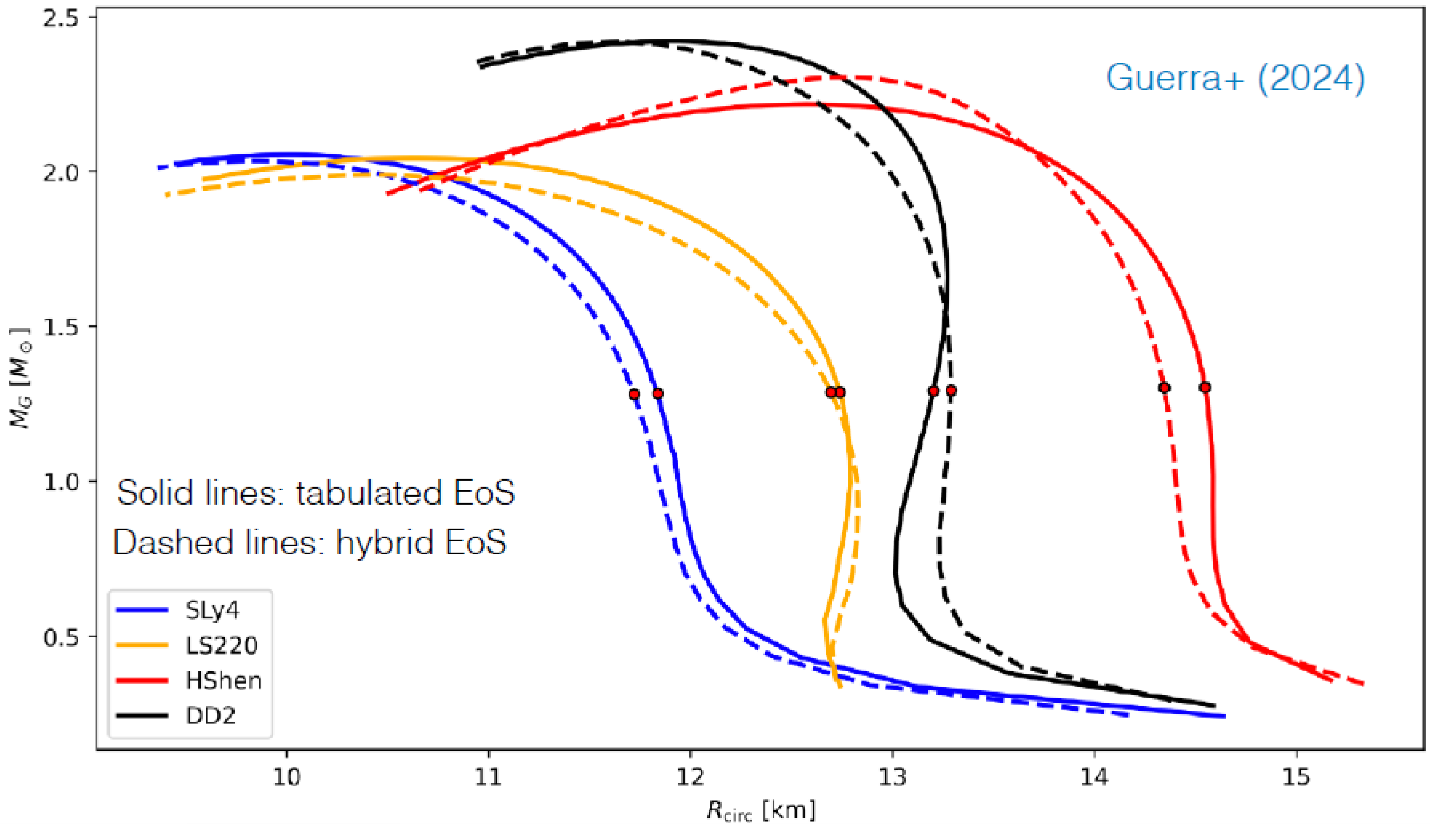

MIRK methods for the RRMHD equations

·· Magnetic fields are key in accretion disks, AGN, relativistic jets, compact objects.

·· A consistent treatment is necessary to avoid numerical resistivity.

·· Hyperbolic equations + constraints (divergence of magnetic and electric fields) → augmented system of hyperbolic equations [Komissarov 2007] (velocity, density, electric and magnetic fields, two additional scalar equations).

·· Structure of the equations:

$$\partial_t E^j = S_E^j - \sigma W[E^j + (v \times B)^j - (v_l E^l) v^j] = \tilde{S}_E^j,$$

$$\partial_t B^j = S_B^j,$$

$$\partial_t Y = S_Y,$$

·· Avoid numerical instabilities due to stiff source term in the evolution equation for the electric field for high conductivities.

MIRK methods for the RRMHD equations

·· PIRK methods to deal with wave-like equations (electric and magnetic fields) for low-order methods.
[I. C.-C. and P. Cerdá-Durán, arXiv:1211.5930 (2012)]
[I. C.-C. and P. Cerdá-Durán, SEMA SIMAI Springer Series Vol. 4 (2014)]

$$\begin{cases} u_t = \mathcal{L}_1(u,v), \\ v_t = \mathcal{L}_2(u) + \boxed{\mathcal{L}_3(u,v),} \end{cases}$$

linearization $\begin{cases} u_t = \bar{\alpha}_1 u + \bar{\alpha}_2 v, \\ v_t = \bar{\gamma}_1 u + \bar{\gamma}_2 v + \boxed{\bar{\lambda} u,} \end{cases}$

wave-like eq.: $(\bar{\alpha}_1 - \bar{\gamma}_2)^2 + 4\bar{\alpha}_2(\bar{\gamma}_1 + \bar{\lambda}) < 0.$

·· Ideal limit: infinite conductivity and $E^i = -(\boldsymbol{v} \times \boldsymbol{B})^i.$

·· Implicit / Semi-implicit methods include additional recoveries of primitive variables from conserved ones [Palenzuela et al. 2009] → potential convergence problems, additional computational cost.

MIRK methods for the RRMHD equations

·· First-order MIRK method (stability criteria to select coefficients):

$$
\begin{aligned}
E^j|_{n+1} &= E^j|_n + \Delta t\, S_E^j|_n - \Delta t\, \overline{\sigma}|_n \left[c_1 E^j|_n + (1-c_1)\boxed{E^j|_{n+1}} + c_2 (v \times B)^j|_n \right. \\
&\quad \left. + (1-c_2)(v|_n \times \boxed{B|_{n+1}})^j - c_3 v^j|_n v_l|_n E^l|_n - (1-c_3) v^j|_n v_l|_n \boxed{E^l|_{n+1}}\right], \\
B^j|_{n+1} &= B^j|_n + \Delta t\, S_B^j|_n, \\
Y|_{n+1} &= Y|_n + \Delta t\, S_Y|_n.
\end{aligned}
$$

→ Pure explicit method with an effective time step:

$$
E^i|_{n+1} = E^i|_n + \frac{\Delta t}{1 + \Delta t\, \overline{\sigma}|_n} \left[S_E^i|_n + \overline{\sigma}|_n E^l|_n \left(v^i|_n v_l|_n - \delta_l^i \right) - \overline{\sigma}|_n (v|_n \times B|_{n+1})^i \right]
$$

·· Analogous derivation for the two-stage second-order MIRK method.

MIRK methods for the RRMHD equations

·· Applications: Self-similar current sheet: 1D problem; CFL=0.8; initial data at t=1:

$$\boldsymbol{v} = (v^x, 0, 0),\ \boldsymbol{E} = (0,0,0),\ \boldsymbol{B} = (0, B^y(x, t=1), 0),\quad B_e^y(x,t) = \operatorname{erf}\left(\frac{x}{2}\sqrt{\frac{\sigma}{t}}\right) \qquad \sigma = 10^3$$

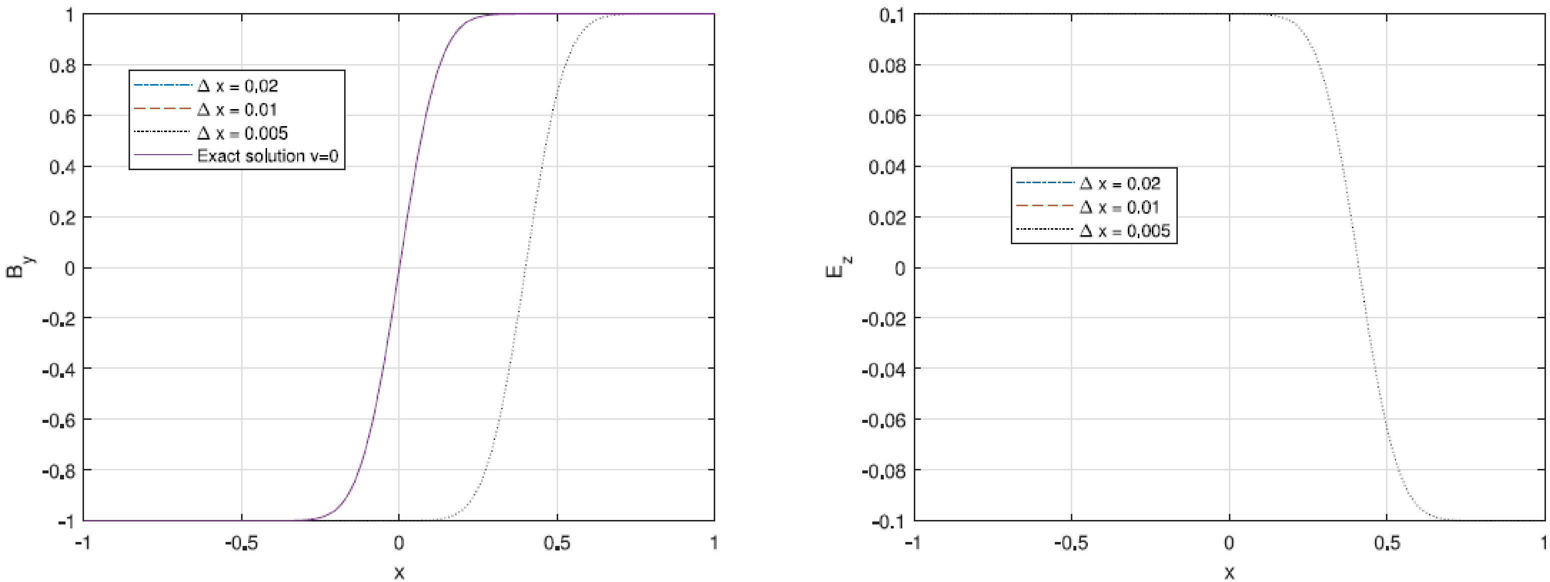

Stable simulations with zero and non-zero velocities ($v_x = 0.1$),
first and second-order methods.

MIRK methods for the RRMHD equations

·· Applications: Circular Polarized Alfvén waves: 1D; full system (including matter); EoS for an ideal fluid, $\Gamma = 4/3$; $\rho(x,0) = p(x,0) = 1$; CFL=0.3 → 0.7; $\sigma = 10^8$; KO term;

$$\boldsymbol{B}(x,0) = B_0\,(1, \cos(kx), \sin(kx)),$$

with $k = 2\pi$ and $B_0 = 1.1547$, and

$$\boldsymbol{E}(x,0) = -\boldsymbol{v}(x,0) \times \boldsymbol{B}(x,0),$$

with $\boldsymbol{v}(x,0) = \frac{v_A}{B_0}(0, B^y(x,0), B^z(x,0))$ and $v_A = 0.423695$

Stable simulations, with first and second-order methods.

Exact solution refers to the one in the stiff limit (close enough for very high conductivities).

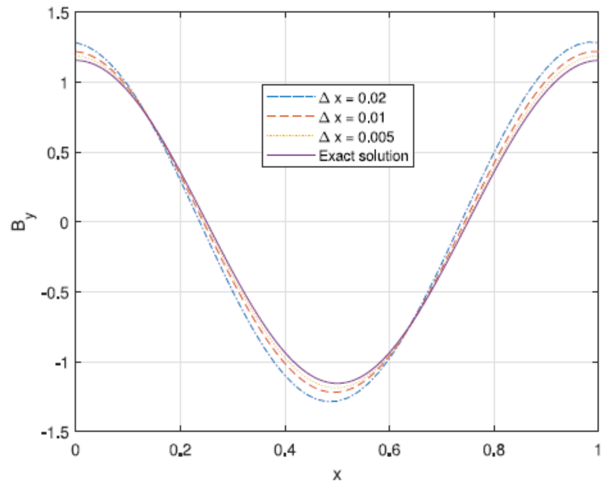

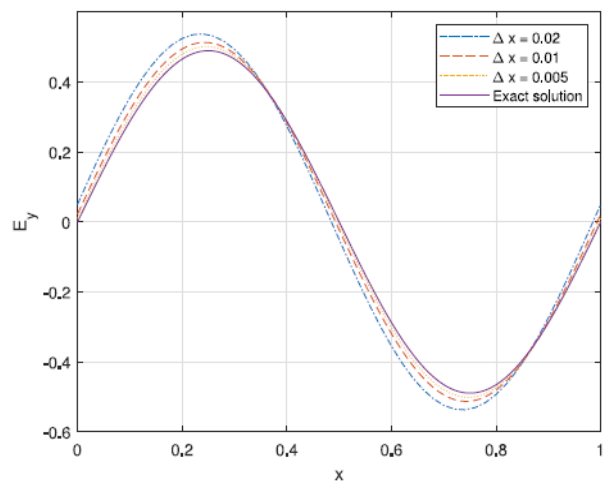

MIRK methods for the M1 neutrino transport equations

·· The explosion mechanism of CCSNe cannot be understood without a detailed account of the generation and transport of neutrinos.

·· Boltzmann equation (7D problem) → momentum-space integration of the distribution function. Truncation: n=0 or diffusion; n=1, quite used – M1 scheme.

·· Optically thick regime → very different timescales of different interactions and stiff source term for very high opacities.

·· Structure of the equations:

$$\partial_t E = S_E + C^{(0)}, \qquad C^{(0)} = c\,\kappa_a (E_{\mathrm{eq}} - \boxed{E}),$$
$$\partial_t F^i = S_F^i + C^{(1),i}, \qquad C^{(1),i} = -c\,\kappa_{\mathrm{tra}} \boxed{F^i}.$$

·· IMEX-like method [Just et al. 2015]. Complexity of applying IMEX methods: opacities, equilibrium profile.

MIRK methods for the M1 neutrino transport equations

·· Similar derivation of MIRK methods, taking into account stability and limit at the stiff limit: effective time-step when written similar to explicit methods.

→ First-order:

$$E^{n+1} = E^n + \frac{\Delta t}{1+\Delta t\,\kappa^n}\left[S_E^n + \kappa^n(E_{\rm eq}^n - E^n)\right]$$

$$(F^i)^{n+1} = (F^i)^n + \frac{\Delta t}{1+\Delta t\,\kappa'^n}\left[(S_F^i)^n - \kappa'^n(F^i)^n\right]$$

→ Second-order: (similar expressions for F)

$$\begin{aligned} E^{(1)} &= E^n + \Delta t\Big[S_E^n + a\,\kappa^n(E_{\rm eq}^n - E^n) \\ &+ (1-a)\,\kappa^n(E_{\rm eq}^n - E^{(1)})\Big], \\ E^{n+1} &= \frac{1}{2}[E^{(1)} + E^n] \\ &+ \Delta t\Big[\frac{1}{2}S_E^{(1)} + a'\,\kappa^{(1)}(E_{\rm eq}^{(1)} - E^{(1)}) \\ &+\frac{1-a}{2}\kappa^{(1)}(E_{\rm eq}^{(1)} - E^n) \\ &+\left(\frac{a}{2} - a'\right)\kappa^{(1)}(E_{\rm eq}^{(1)} - E^{n+1})\Big], \end{aligned}$$

Opt 1) Second order at the stiff limit for smooth variables:

$a' = \dfrac{a-1}{2}$ (similar for b').

Opt 2) Guarantee of stiff limit even if non-smooth variables:

$b' = \dfrac{(1-b)^2}{2b}, \quad b \in (-\infty, 0) \cup (1/2, 1)$ (similar for a').

MIRK methods for the M1 neutrino transport equations

·· Applications: Simple test: test 1 from [J.A. Pons, J.M. Ibáñez, J.A. Miralles, MNRAS 317, 550-562 (2000)]:

Difussion limit (P = p E = E/3) in spherical symmetry (1D problem) and $\kappa_{\rm a} = 0$:

$$\partial_t E + \partial_r F + \frac{F}{r} = -c\, \cancelto{0}{\kappa_{\rm a}} \left(E_{\rm eq} - E\right)$$

$$\partial_t F + \partial_r P + \cancelto{0}{\frac{3P - E}{r}} = -c\, \kappa_{\rm tra} F$$

Analytical solution, c=1 (geometrical units):

$$E(t,r) = \left(\frac{\kappa_{\rm tra}}{t}\right)^{3/2} \exp\left(-\frac{3\kappa_{\rm tra} r^2}{4t}\right) \qquad F(t,r) = \frac{r}{2t} E(t,r)$$

MIRK methods for the M1 neutrino transport equations

·· Applications: Simple test:
MIRK1: a=b=0. MIRK2: a=b=1/2, a'=(a-1)/2, b'=(b-1)/2. Similar results.

0.6302	0.7416	0.8401	0.9096	0.9516	MIRK1	4.1606	1.4709	1.7560	1.9217	1.9835
0.6308	0.7424	0.8409	0.9102	0.9520	MIRK2	4.1602	1.4704	1.7553	1.9202	1.9804

Numerical flux: Godunov method

$\kappa_S = 10^2, \quad t = 5$

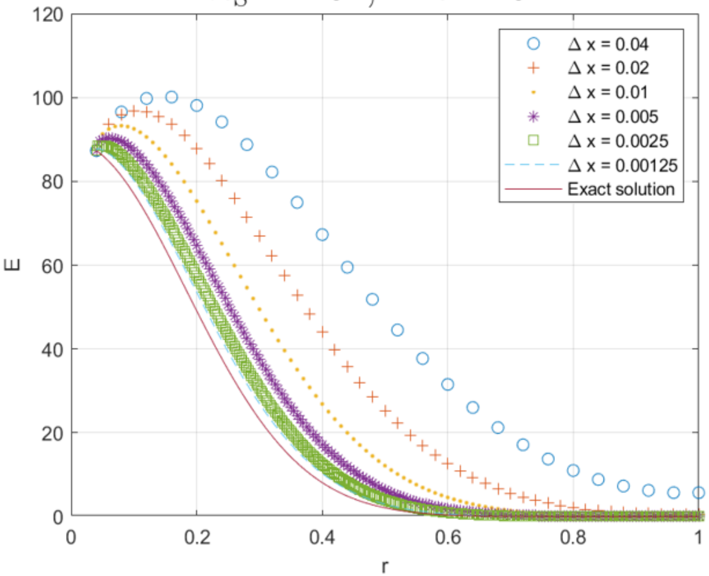

Numerical flux: Centered finite differences

$\kappa_S = 10^5, \quad t = 500$

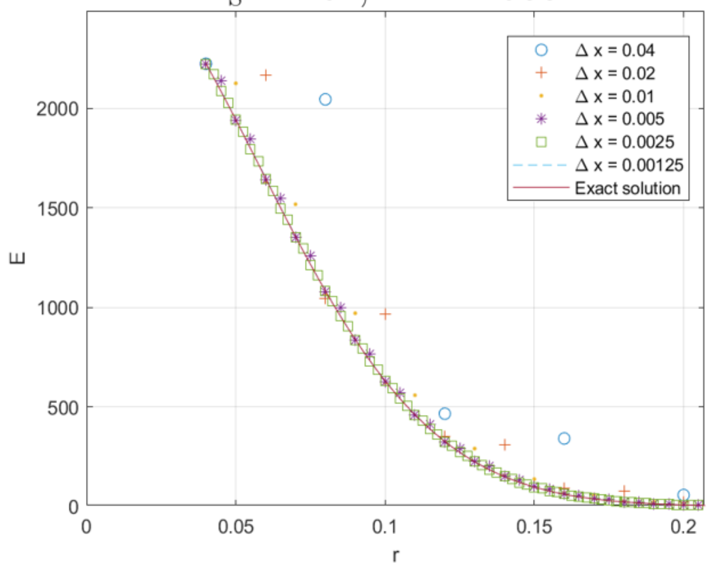

CFL=1.

Exact solution used at boundary conditions and initial data at t=1.

MIRK methods for the M1 neutrino transport equations

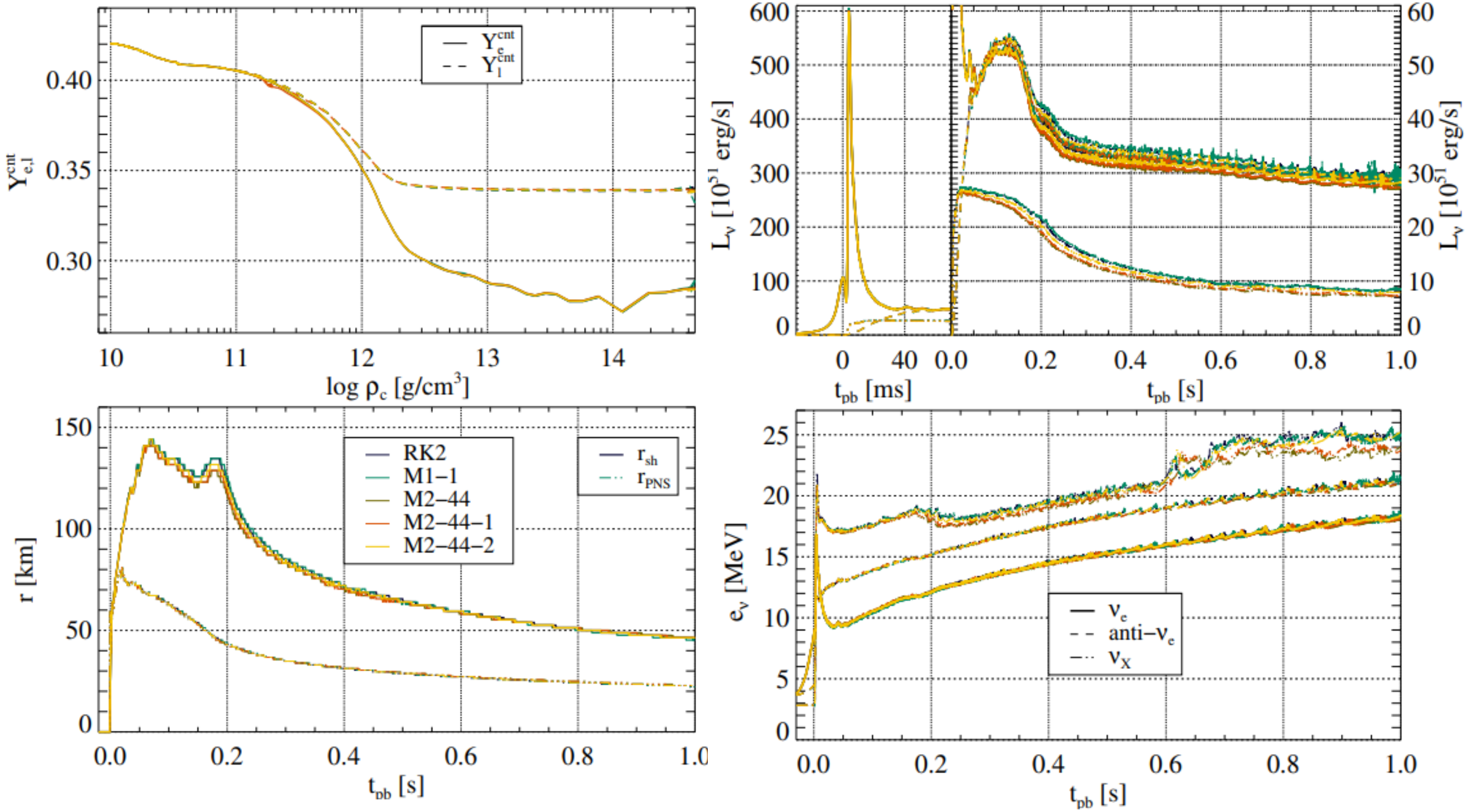

·· Applications: Core-collapse simulation with all the important interactions that dominate the dynamics (see more details in arXiv reference).

MIRK methods for the M1 neutrino transport equations

·· Applications: Core-collapse simulation:

→ Stable and accurate results using 1st and 2nd MIRK methods vs reference.
→ Direct relation between the values of the coefficients and stability + correct values at the stiff limit (non-smooth variables).
→ Slight modifications from pure explicit methods and similar computational cost, independently of the complexity of opacities and equilibrium profile.

General idea MIRK methods: Hyperbolic equations with stiff source terms that can be somehow linearized with respect to the conserved (evolved) variables:

$$\partial_t U + \partial_i F^i(U) = S(U), \qquad S(U) = S_E(U) + \frac{1}{\epsilon}[S_I(U) - U_0];$$

$$S_I(U) = \sum_{i=1}^{n} G_i(U) \boxed{U^i}.$$

Only the conserved variables are evaluated implicitly. More examples: GR force-free electrodynamics, rarefied gases problems, shallow water equations with friction...

Constrained evolution schemes: SOLVE the evolution and constraint equations on each spatial hypersurface: CFC, FCF...

CFC (Conformally Flat Condition) Isenberg 1979/2008, Wilson and Mathews 1989: conformally flat spatial 3-metric; gravitational radiation encoded in the neglected terms.

· Exact in spherical symmetry (CC 2011). Very accurate for axisymmetric rotating NSs.

· Set of elliptic equations for the metric variables (including the constraint equations): lapse, shift, conformal factor.

· Shares similar structure with XCTS, used in generation of initial data.

· Original formulation suffers from a non-local uniqueness pathology at extreme curvature or very high density regimes. This problem is solved with the introduction of auxiliary variables [Cordero-Carrión et al., 2009]. See talk in Einstein toolkit meeting 2019.

FCF (Fully Constrained Formulation) Bonazzola et al., 2004:
· Maximal slicing and Dirac generalized gauge.
· Similar elliptic system as in CFC with additional source terms + hyperbolic new sector encoding the GW radiation.

Elliptic equations are more stable but difficult to solve and parallelize:
· Initial data talk by P. Grandclément → spectral methods with Lorene library, commonly used.
· Chevishev-Jacobi methods (CJM) (Adsuara et al. 2017): parallelization is possible.

Hyperbolic equations: PIRK methods developed for the hyperbolic FCF sector and afterwards applied to other (free evolution) formulations (BSSN).

Coupled with matter content...

Black hole singularities: infinite quantities cannot be treated numerically

→ Remap somehow your space-time: punture method commonly used in free evolution schemes (BSSN) and BBH simulations.

→ Excise a topological sphere from your numerical grid containing the black hole singularity:

· Pretorius 2005 simulations used GHG and excision.

· Excision can be combined with the CFC formulation [Cordero-Carrión et al., 2014].

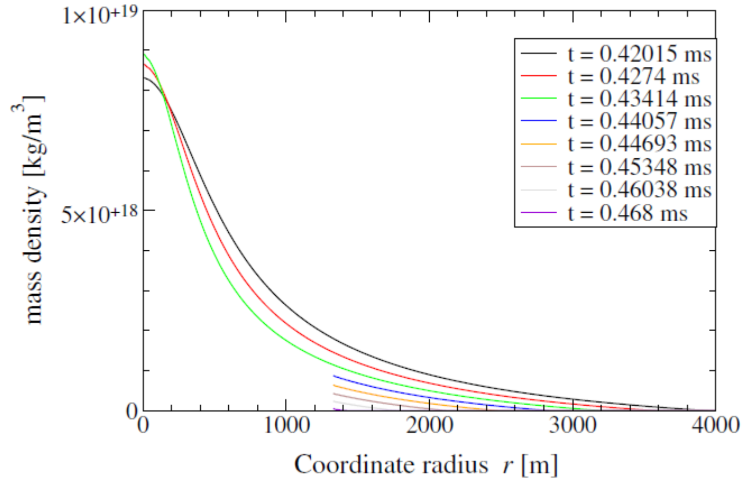

This idea with a small modification has been recently used in core-collapse simulations [B. Sykes et al., 2023].

More ideas are about to come in the 1D case.

More research is needed in the 2D / 3D cases.